Hindawi
Complexity
Volume 2019, Article ID 2096749, 16 pages
https://doi.org/10.1155/2019/2096749

Research Article

A Century of Topological Coevolution of Complex Infrastructure Networks in an Alpine City

Jonatan Zischg,[1] **Christopher Klinkhamer**,[2] **Xianyuan Zhan**,[3] **P. Suresh C. Rao**,[2] **and Robert Sitzenfrei**[1]

[1] *Unit of Environmental Engineering, Department of Infrastructure, University of Innsbruck, Technikerstrasse 13, 6020 Innsbruck, Austria*
[2] *Lyles School of Civil Engineering, Purdue University, 550 Stadium Mall Drive, West Lafayette, IN 47907, USA*
[3] *Urban Computing Business Unit, JD Finance No. 18 Kechuang 11 Street, Beijing, China*

Correspondence should be addressed to Jonatan Zischg; jonatan.zischg@uibk.ac.at

Received 24 May 2018; Revised 29 November 2018; Accepted 3 December 2018; Published 6 January 2019

Academic Editor: Albert Diaz-Guilera

In this paper, we used complex network analysis approaches to investigate topological coevolution over a century for three different urban infrastructure networks. We applied network analyses to a unique time-stamped network data set of an Alpine case study, representing the historical development of the town and its infrastructure over the past 108 years. The analyzed infrastructure includes the water distribution network (WDN), the urban drainage network (UDN), and the road network (RN). We use the dual representation of the network by using the Hierarchical Intersection Continuity Negotiation (HICN) approach, with pipes or roads as nodes and their intersections as edges. The functional topologies of the networks are analyzed based on the dual graphs, providing insights beyond a conventional graph (primal mapping) analysis. We observe that the RN, WDN, and UDN all exhibit heavy tailed node degree distributions [$P(k)$] with high dispersion around the mean. In 50 percent of the investigated networks, $P(k)$ can be approximated with truncated [Pareto] power-law functions, as they are known for scale-free networks. Structural differences between the three evolving network types resulting from different functionalities and system states are reflected in the $P(k)$ and other complex network metrics. Small-world tendencies are identified by comparing the networks with their random and regular lattice network equivalents. Furthermore, we show the remapping of the dual network characteristics to the spatial map and the identification of criticalities among different network types through co-location analysis and discuss possibilities for further applications.

1. Introduction

Many complex systems can be described as networks [1], and with recent increases in computing power it is now feasible to investigate the topologies of entire networks consisting of high-resolution data [2]. Examples of these types of investigations range from molecular interaction networks (e.g., protein interactions of cells) and social networks (e.g., communication between humans) to global transportation systems and individual human mobility [3–6].

Despite the differences in various types and representations of these networks, important commonalities exist. The analysis of complex networks gives insight to structural morphologies, similarities, recurring patterns, and scaling laws [7, 8]. The applications are multifaceted: identification of central nodes; prediction of future developments and network growth; information transfer; identification of vulnerabilities to enhance security [9]; and improvement of network resilience [10, 11]. Complex network analyses of critical infrastructure, such as water distribution networks (WDNs) and urban drainage networks (UDNs), provide valuable insights beyond the traditional engineering approaches, to design and operate systems in a more reliable way and to help build-up structural resiliency [12, 13].

In the past, most structural features in complex networks were investigated based on a conventional graph representation (so-called "primal space"), where pipes or conduits are the edges and their intersections the vertices

of a mathematical graph [14, 15]. Conversely, different approaches, based for example on common attribute classification (i.e., road name or pipe size) or intersection continuity (i.e., maximum angle of deflection), consider the network structure in its "dual space", i.e., functional components (e.g., pipes with same diameter) which belong together, represent the vertices and their intersection the edges of the graph [16, 17]. Further explanations are provided in the next section. Unlike the conventional primal representation, dual mapping approaches may also consider the continuity of links (pipes or conduits) over a variety of edges and hierarchy (e.g., pipe diameter; isolation valves; maximum designed flow; speed limits; road class) for further graph analysis.

There exist different ways of creating the dual graph of a network, taking into account physical (e.g., geometric) and/or behavioral (e.g., symbolic) considerations. The street name (SN) approach, for example, uses the historical naming conventions to create the dual graph, but neglects the geometrical properties of the network. Hybrid approaches, like the Hierarchical Intersection Continuity Negotiation (HICN) [16], combine geometric (e.g., maximum angle of deflection of connected roads) and hierarchical (e.g., road class) attributes, to better capture the structural network topology resulting from top-down (centralized designs) and bottom-up local-planning actions (self-organization).

Previous studies using the dual mapping approach were mainly performed on road networks (RNs) [16–18], but some also on water distribution and urban drainage networks [19–21]. In principle, an extension to each network type is possible. Masucci et al. [16] investigated the road network growth for the city of London and found stable statistical properties to describe the topological network dynamics. Krueger et al. [20] applied the HICN principle for the first time to the evolving sewer networks in a large Asian city with 4 million people. The authors found that sewer network types quickly evolve to become scale-free in space and time. In Jun and Loganathan [19] a dual mapping approach was used to describe the connectivity of isolation zones in water distribution networks.

Klinkhamer et al. [21] examined the co-location of existing road and sewer networks in a large Midwestern US city and homoscedasticity of subnets across the city but did not examine temporal evolution of these networks. In Mair et al. [22] the geospatial co-location of roads, pipes, and sewers was investigated using data set for three Alpine case studies, finding strong similarities between these networks. Studies on the coevolution of water infrastructure networks (water distribution and urban drainage) and road network are crucial when investigating functional interdependencies and cascading vulnerabilities across multiplex network layers. Examples are the flood-induced change in road traffic or the collapse of entire road segments causing flow disruptions in all networks to different extents.

In this paper, we present for the first time a topological analysis of three infrastructure networks coevolving over a century. The results of the dual mapping for a unique dataset of 11 time-stamped water distribution and urban drainage network states and 8 time-stamped road networks of the medium-size Alpine case study city, as the town and its infrastructure, evolved during the past 108 years, and the population tripled from about 40,000 to about 130,000. First results of this case study are presented in Zischg [23]. We investigated network topological metrics using the HICN dual mapping approach [16]. We observe that some infrastructure networks show node degree distributions that behave like truncated power-laws under the dual representation. However, this "scale-free" network characteristics depend on the network type and change over time. With the presented methodology, differences and similarities of patterns (e.g., vertex connectivity) and trends for the infrastructure development are obtained. This study includes an investigation of the sensitivity of the dual mapping approach, using different criteria to build the new graph. The reflected structural features, such as the backbone of the networks, were uncovered for each network type and remapped to the spatial map. A further analysis shows the pairwise co-location of high node degree components ("network hubs") across different infrastructure network types, which builds the basis for analyzing disturbances and structural resilience.

2. Data Analyses

2.1. Network Connectivity. Node degree distribution $P(k)$ is a significant topological property of complex networks. The degree (k) of a node i in an undirected network describes the number intersecting links and is calculated through the network's adjacency matrix A, where the degree of node i is defined by the sum of the i-th row of A. For example, the node degree in social networks represents the number of contacts. Scale-free networks show node degree distributions that follow a Pareto power-law distribution [20, 21], with $P(k) \sim k^{-\gamma}$ for $k \geqslant k_{min}$, whereas random networks have Poisson distributed node degrees. We use the method proposed by Clauset et al. [24] to test the power-law hypothesis and determine scaling parameters of the node degree distributions for the various network states. By calculating the p value, an indicator for the goodness-of-fit is determined. In case the p value is greater than 0.1, the power-law is a plausible hypothesis for the data within given ranges. However, the definitive recipe to fit power-law distributions does not yet exist [25]. The mean node degree for undirected networks is defined as $\langle k \rangle = (2 \times e)/n$, where e is the total number of edges and n is the total number of vertices. In the limits a mean node degree of 2 indicates a tree-like network structure, and grid patterns or cyclic structures have mean node degrees around 4 [26]. Higher statistical moments of $P(k)$ are also important, including the variance $\langle k^2 \rangle$ that reflects the dispersion around the mean [27].

Along with the node degree distribution, the characteristic path length $\langle l \rangle$ (or average path length) is an important and robust measure of network topology. It quantifies the level of integration/segregation throughout the network. In water infrastructure and power grid networks energy losses are dependent on the characteristic path length. It is calculated by the average shortest path distance between all couples of nodes as follows:

$$\langle l \rangle = \frac{1}{n \times (n-1)} \times \sum_{i \neq j} d\left(v_i, v_j\right), \quad (1)$$

where n is the number of vertices and $d(v_i, v_j)$ denotes the shortest path between vertex v_i and v_j [3]. The probability density function of the shortest path lengths (between all couples of nodes for RNs; between all terminal nodes and the source or sink node, for WDNs and UDNs, respectively), $P(l)$ can, for example, be considered as the approximation of the travel-time distribution with a nearly consistent distribution of flow velocities.

The local clustering coefficient C_i of node i describes the connectivity (number of edges m) among its k neighbors. A perfect cluster/clique ($C_i = 1$) indicates a full connection of all nodes/individuals. If an isolation of one node in the cluster occurs, the other nodes remain connected. Conversely, a $C_i = 0$ indicates that node i holds together all its neighboring nodes. Regarding infrastructures, a higher clustering coefficient indicates the existence of local and alternative flow paths in the network. In undirected graphs, C_i for an individual node is defined as follows:

$$C_i = \frac{2 \times m}{k_i \times \left(k_i - 1\right)}. \quad (2)$$

The overall (average) clustering coefficient C can be determined by averaging the local clustering across all nodes. When the network reveals a high C, which is typical for regular lattice networks (high local efficiency), and has a small $\langle l \rangle$, as found in random networks (high global efficiency), then the network can be characterized as small-world network [30]. Telesford et al. [31] developed methodology to test the "small worldness" by comparing the network with its equivalent random and regular lattice networks, which have the same node degree distribution, as follows:

$$\omega = \frac{\langle l_R \rangle}{\langle l \rangle} - \frac{C}{C_L}, \quad (3)$$

where $\langle l_R \rangle$ is the characteristic path length of the randomized network equivalent and C_L is the clustering coefficient of the regularized network equivalent. A ω-value of 0 indicates a network that is in perfect balance between normalized values of high clustering and low characteristic path length. Negative values indicate a graph with more regular characteristics, whereas positive values indicate more random graph characteristics [31]. Small-world networks are significantly more clustered (segregated) than random networks and have the same characteristic path length as random (integrated) networks, making them locally and globally efficient, for example, for optimal information transfer [30].

2.2. HICN Principle for Dual Mapping. The HICN approach emphasizes the functional topology of the network by aggregating components (e.g., pipes, conduits, and roads) with identical attributes (e.g., pipe diameter, pipe segments, and road type), while also maintaining a certain level of straightness (e.g., road sections) [16]. After reducing the network complexity with this "generalization model," the aggregated edges are converted into vertices and the intersections are converted into edges. The resulting graph is the so-called "dual" (mapped) representation of the "primal" graph (see Figure 1). In addition to the edge class, the angular threshold Θ_{max} is a second criterion used for the generalization model. It defines the maximum exterior convex angle of connected edges being merged [17].

The HICN allows for reducing the network complexity of the primal map and considers the hierarchy of network elements (e.g., different level of detail of the pipe representation). Identical cohorts of edges are considered as a single component, the dual node. However, the dual mapped network circumvents this issue through generalization and still preserves the connectivity information of the original network. Another advantage is the detachment from the geographical embedding, allowing the network to be nonplanar. With this methodology, the underlying hierarchy (e.g., highly connected components) of the network can be uncovered.

3. Alpine Case Study

To investigate the coevolving topology of three urban infrastructure networks with the HICN dual mapping methodology, we utilize available, high-resolution network data for a medium-size Alpine city. The temporal evolution of the urban infrastructure networks is defined through time-stamped system states at 10-year intervals, starting with the year 1910 for water distribution and urban drainage networks. The road network data starts with the year 1940, since historical orthophotos to reconstruct the network were only available from that time. The city has grown from approximately 40,000 inhabitants in 1910 to 130,894 in 2016. The historical data set describes the expansion of the networks and includes pipe rehabilitation, changing source (e.g., reservoirs), and sink nodes (e.g., sewer outfalls), altering population densities and variations of water consumption patterns of the water distribution and urban drainage systems. The detailed description of the network reconstruction for this case study can be found in the works of Sitzenfrei et al. [32] and Glöckner [33].

Figure 2 shows the time-stamped networks at selected stages in the primal map. For the UDN a greater thickness and a darker color of the edges indicate a larger conduit size, which connect to one large (biological) waste water treatment plant (WWTP) in the eastern part of the city after the 1970s. Before the wastewater was discharged to the river after mechanical treatment (sedimentation, rack), outside the urban areas at the eastern parts of the city. When actually building the WWTP, there were no major changes in the combined drainage network necessary (combined transportation of sewage and storm water) and the old outlets were transferred to combined sewer overflows (CSOs). For security reasons the pipe diameter for the WDN cannot be shown. The color shading at the road network in 2010 indicates the different road types, ranging from residential (light grey), tertiary, secondary, and primary roads to motorways (black). Furthermore, the water demand which directly influences the flows of the WDN and the UDN during dry weather periods is illustrated. Clearly noticeable is the general

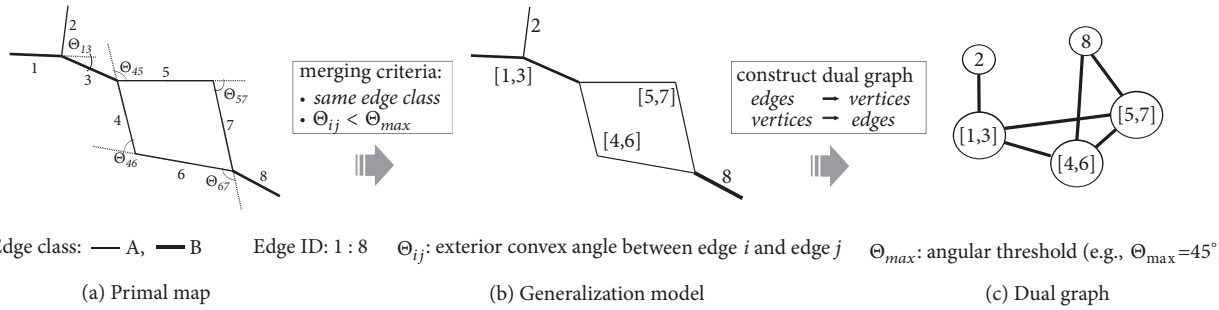

Figure 1: HICN method to construct the dual graph from the primal map. Resulting dual graphs are dependent on the generalization model (adapted from Zischg et al. [28] with permission from ASCE).

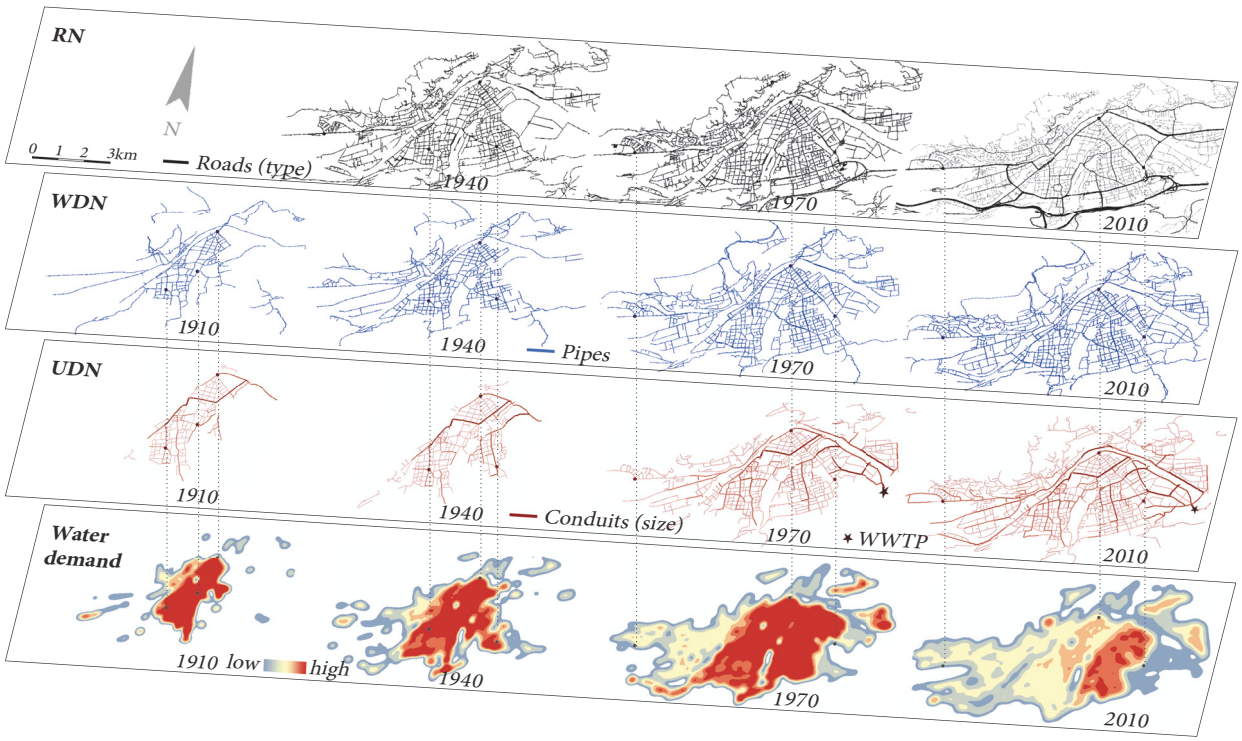

Figure 2: Time-stamped coevolution of the water distribution network (WDN), the urban drainage network (UDN), and the road network (RN) of an Alpine city.

reduction of the average water demand after the 1970s mainly due to water saving measures.

Table 1 gives a short narrative introduction on the history of the infrastructure networks of the investigated case study during the last century.

4. Results and Discussion

In this section, we present the results of the historical coevolution in the dual representation of the three infrastructure networks (WDN, UDN, and RN). In a sensitivity analysis of the HICN method, we determine the effects on $P(k)$ based on the variations of the angular threshold, the edge class, and the network partition (entire network vs. largest connected component (LCC)), before we present the development of the network characteristics over time. Finally, we also show the remapping of dual network characteristics to the primal map, investigate correlations between dual node degree and edge class (e.g., road type), and identify pairwise spatial co-locations of dual nodes among the three network types.

4.1. Dual Mapping. The application of the HICN dual mapping to the historical infrastructure networks for the first (year 1910 for WDN and UDN, and 1940 for RN) and last stages (year 2010) is illustrated in Figure 3. The dual graphs show the node degree (darker and larger nodes represent central network "hubs" with high node degree). For the application of the HICN method to the water infrastructure networks, we used identical pipe diameters (for WDN) and conduit sizes (for UDN) for the edge class criterion, in combination with an angular threshold Θ_{max} of 180 degrees; i.e., we ignore the curvature of pipe/conduit segments. On the

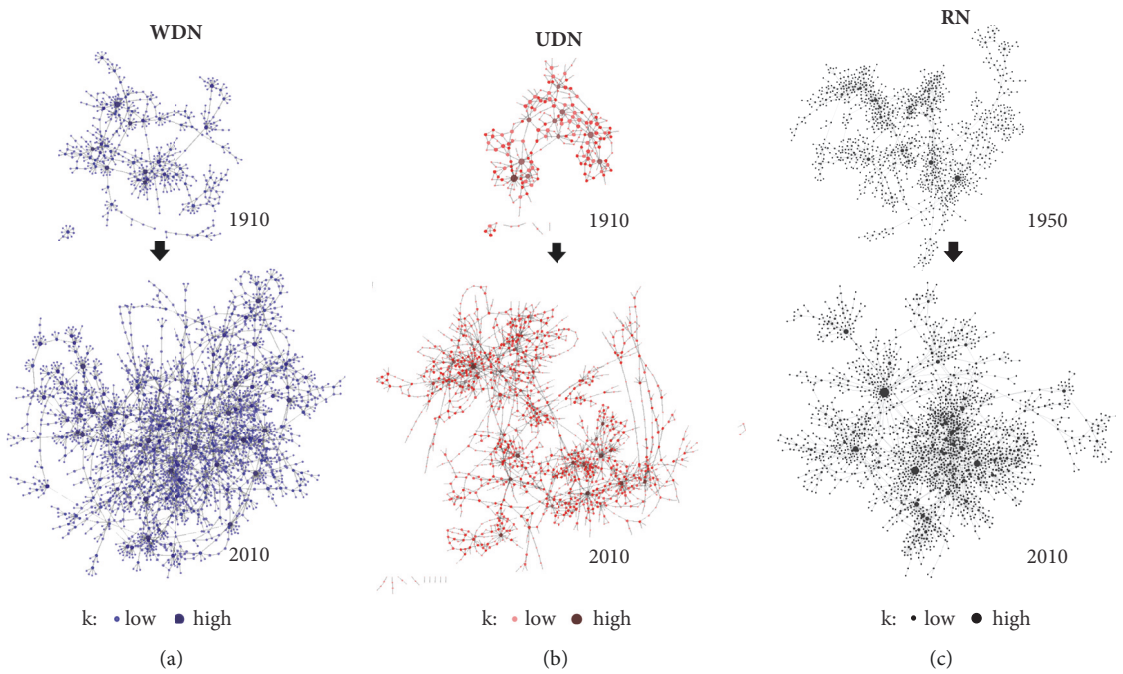

Figure 3: Dual mapped evolution of the infrastructure networks: (a) WDN, (b) UDN, and (c) RN. The color shading and size of the node indicates its degree. The network visualization was done using the program Cytoscape [29].

Table 1: Narrative changes of the infrastructure networks [32–34].

Years	Narrative
Before 1910	WDN for about 23,000 inhabitants; total population 49,727 in 1900; design demand 150 liters per capita and day, transporting a significant amount of water in the city; also the massive amount of waste water had to be transported out of the city by a newly build combined sewer system; a mandatory connection of the consumers to both networks was enforced by law
1910-1929	1st world war; maximum recorded water consumption of 500 liters per capita and day in 1927 due to unaccustomed consumer behavior (still used to the central supply of running wells); 30% of the current WDN structure (year 2017) existed already in 1910; opening of the airport at the eastern part of the city in 1925
1930-1949	2nd world war; massive influx of refugees, infrastructure mainly unaffected; opening of a new airport at the western part of the city in 1948; supply deficits; reduction of water consumption below 300 liters per capita and day through information campaigns
1950-1969	Strong population growth, city and road network expansion; construction of the WWTP (mechanical treatment) in 1966; strong UDN expansion in western and eastern direction; biggest growth rates for the WDN between 1960 and 1970.
1970-1989	380 liters per capita and day; construction of the motorway and connection with the city (1970s); construction of the biological treatment at the WWTP in 1974; connection of neighboring villages to the WWTP; maximum loads of 330,000 people equivalents (PE) in 1987; production industries with high water demand and waste water accumulation leave the city
1990-2009	Further connection of neighboring villages; expansion of the WWTP to 400,000 PE; minor network expansions, increased pipe and sewer rehabilitation
2009-present	Steady population growth, urban expansion is limited by the topographic boundary conditions; densification of city districts (from detached houses to apartment blocks); approximately 250 liters per capita and day (domestic water demand is app. half of it); actually connected people equivalent to the WWTP: 270,000 PE (2011); roads: 476 km; WDN: 320 km; UDN 244 km.

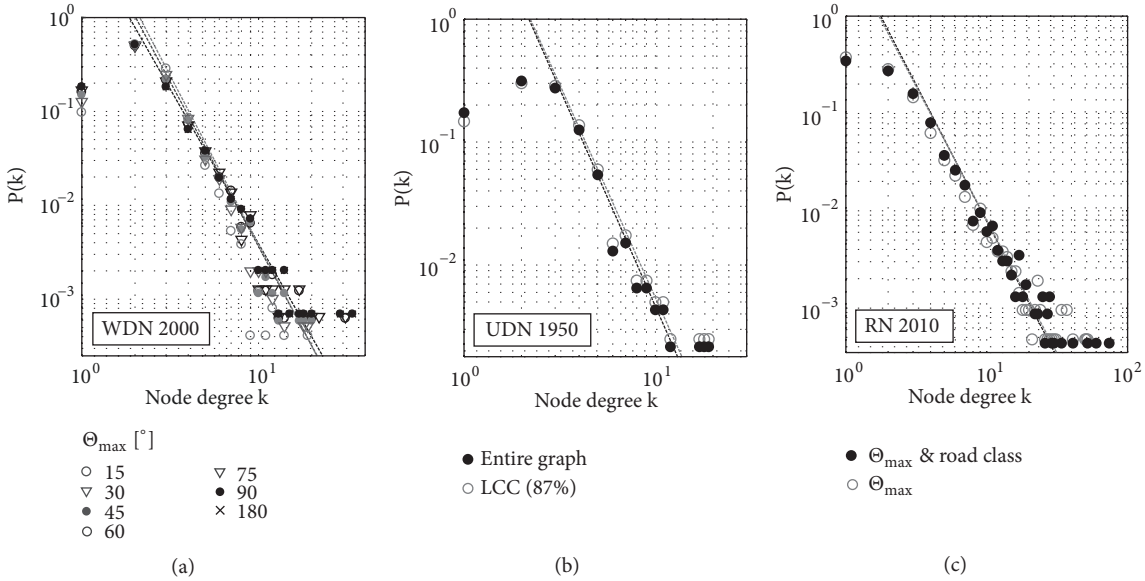

Θ_{max}[°]:	15	30	45	60	75	90	180
n	3,050	2,393	2,102	1,972	1,887	1,764	1,764
γ	5.00	4.09	3.80	3.70	3.61	3.39	3.39
k_{min}	4	3	3	3	3	3	3
p-value	0.000	0.000	0.015	**0.146**	**0.441**	**0.269**	**0.257**

(d)

	Entire graph	LCC
n	462	401
γ	3.57	3.50
k_{min}	3	3
p-value	**0.348**	**0.222**

(e)

	Θ_{max} & road class	Θ_{max}
n	2,295	2,094
γ	2.72	2.66
k_{min}	3	3
p-value	**0.694**	**0.309**

(f)

Figure 4: Parameter sensitivity of the HICN approach on the node degree distribution of the WDN 2000; the UDN 1950 and the RN 2010 (n: number of dual nodes, γ: power-law exponent, k_{min}: lower bound to the power-law behavior, p value: *goodness-of-fit* for the power-law hypothesis).

other hand, for the dual mapping of the road networks, we used the Θ_{max} of 45 degrees [35] and the road type (residential road to motorway) as criteria for the generalization model. We discuss the application of different parameter values in the next section.

4.2. Sensitivity of the Dual Mapping. For the HICN approach different angular thresholds and edge attributes can be considered to construct the dual graph. In Figure 4 we show the results of the sensitivity analysis on the node degree distribution for three parameters used for the HICN approach. First, we identify the sensitivity of the angular threshold Θ_{max} using the WDN of 2000 as reference. Second, we choose the UDN 1950 with 10 subnetworks and investigate the graph characteristics for the entire network and the largest connected component (LCC) only. Finally, we show the effect of neglecting the edge class criterion (road type) for the RN in 2010 as reference.

With increasing angular threshold Θ_{max} (see Figure 1) and the associated less strict criterion for aggregation of edges, we observe that more pipes (of the same class) are merged together and therefore the size of the dual graph is reduced (see Figure 4(a)). For example, the reference network has 7,827 edges in the primal space, which are generalized to 3,050 and 1,764 dual nodes for angular thresholds of 15 and 180 degrees, respectively. Figure 4(d) shows the outcome of 7 variations of the angular threshold Θ_{max} from 15 to 180 degrees. All resulting node degree distributions are heavy tailed and by visual inspection relatively similar. However, when applying the method to test the power-law hypothesis as proposed by Clauset et al. [24], only for $\Theta_{max} > 45$ degrees Pareto distributions $P(k) \sim k^{-\gamma}$, $k \geq k_{min}$ are plausible data fits (p value ≥ 0.1). At this point it should be mentioned that power-law fitting is still a controversial issue and a definitive recipe to fit power-law distributions and to distinguish between power-law and power-law-like distributions does not yet exist [25]. A minimum node degree k_{min} of 3 for curve fitting was determined to be the most likely one, for all three network types. For higher threshold angles slightly decreasing slopes γ are observed. The results using angular thresholds of 90 and 180 degrees are identical, meaning that no sharp inner angles between connected pipes of the same class are found in the graph. Unlike for road networks, where Θ_{max} also is a criterion for visibility and navigation, we suggest that restricting Θ_{max} in WDNs and UDNs is less important to find and aggregate pipe segments with unique identity because of their underground locations. We conclude that for investigating the node degree distribution of the historical networks, the angular threshold Θ_{max} is of minor importance, but must be consistently applied between the types and the states of the networks.

Figure 4(b) shows the results when investigating the entire graph (all subnetworks) and the largest connected component (LCC), which contains 87% of the total nodes.

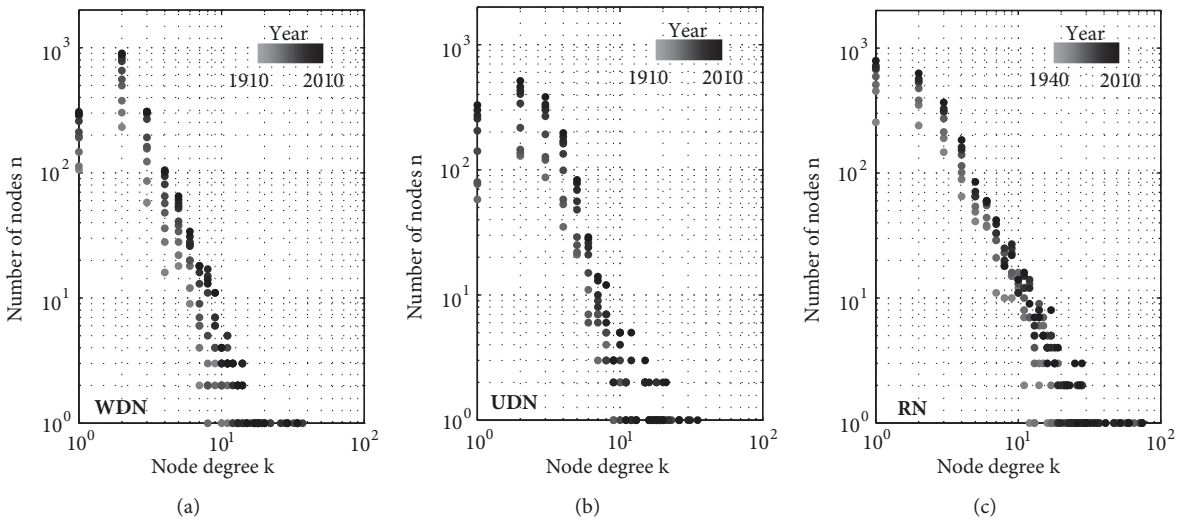

Figure 5: Heavy tailed dual degree distribution overtime of (a) the WDN, (b) the UDN, and (c) the RN. The color shading from light grey to black indicates the evolution of the network. Detailed results of the statistical curve fitting can be found in Appendix A.

For the reference network UDN 1950, no significant changes in the Pareto exponent are seen (see Figure 4(e)). Finally, the neglect of the road class as additional criterion for the HICN method slightly decreases the size of the network but has a low effect on the probability density function $P(k)$ (see Figures 4(c) and 4(f)). This can be interpreted with the low incidence of changing road types across straight road segments.

In this study, we used the pipe diameter to identify functionally identical pipe segments. Other examples could be the age or the material of the pipe, but also classified (design) flows or (measured or modeled) head losses might be used to construct the dual graph. The advantage of using the pipe diameter is that it is a surrogate measure of the flow and is independent of a hydraulic simulation. The black dots in Figure 4 represent the network configuration as presented in the subsequent section.

4.3. Characteristics of the Dual Graph. Resulting node degree distributions, $P(k)$, for the WDN, UDN, and RN in the dual representation are presented in Figure 5, plotted for all network types on log-log axes for the time-stamped states. A darker node color indicates a younger and more mature network state. We observe heavy-tailed node degree distributions for 30 network states with dispersion indices D ($\langle k^2\rangle/\langle k\rangle$) > 1, indicating high variance around the mean. Detailed analyses showed that 50% of the time-stamped networks follow truncated power-law [Pareto] distributions across all network types. This does not necessarily mean, however, that alternative (e.g., log-normal, exponential) distributions are more plausible. The scaling parameters γ fall in the range between 3.23 and 3.50 for WDN ($k_{min} = 2$ or 3), 3.25 and 3.76 for UDN ($k_{min} = 3$ or 5), and 2.67 and 2.78 for RN ($k_{min} = 3$). For the WDN (mean: 3.35 ± 0.09) and UDN (mean: 3.49 ± 0.12) larger slopes γ and a stronger decrease of the number of leaf nodes ($k = 1$) are found compared with the RN (mean: 2.70 ± 0.04). A possible explanation of the truncation could be the missing house (low degree) connections for both water infrastructure networks. For the detailed parameters and the statistical tests, we refer to Appendix A.

The truncated power-law [Pareto] distribution also indicates that the probability of finding nodes with many connecting links ("hubs") is much lower than of nodes with few connections (terminal dual nodes). According to the literature this behavior is typical for scale-free networks, which are dominant in most natural networks. The extent to which these distributions fit a power-law can be a useful marker of network resilience [36].

The "scale-free" similar characteristics, within the observed range [$k_{min} \leqslant k \leqslant k_{max}$], are also indicated with the significant higher maximum degrees k_{max} (representing a "network hub") compared to the mean degree $\langle k\rangle$ (see Appendix B). Although the mean degree $\langle k\rangle$ of the UDN is larger than that for the WDN, the maximum degree k_{max} of both water infrastructure networks is similar. One reason for that is fewer changes in the conduit diameters, resulting in the aggregation of more conduits and thus having higher connectivity. The highest connectivity and dispersion index D is found for the road network, indicated by high k_{max} and high $\langle k^2\rangle/\langle k\rangle$ (see Appendix B and Figure 6(c)).

The growth of the networks in terms of total number of dual nodes n over time is illustrated in Figure 6(a). Highest growth rates of the networks are seen in the 1960s and 1970s, which can be partly related to the economy boom and the implementation of the waste water treatment plant [32]. Figure 6(b) presents the scaling parameter γ of the node degree distributions $P(k)$ over time. A change in the lower bound k_{min} is indicated in round brackets. Although the power-law hypothesis could only be clearly proven in 50% of the time-stamped networks (see Appendix A), we show the scaling parameter for all network states for comparison purposes. The statistical analysis shows that the RN tends towards a clear scale-free behavior during evolution, whereas the opposite is observed for the UDN. No clear trends were

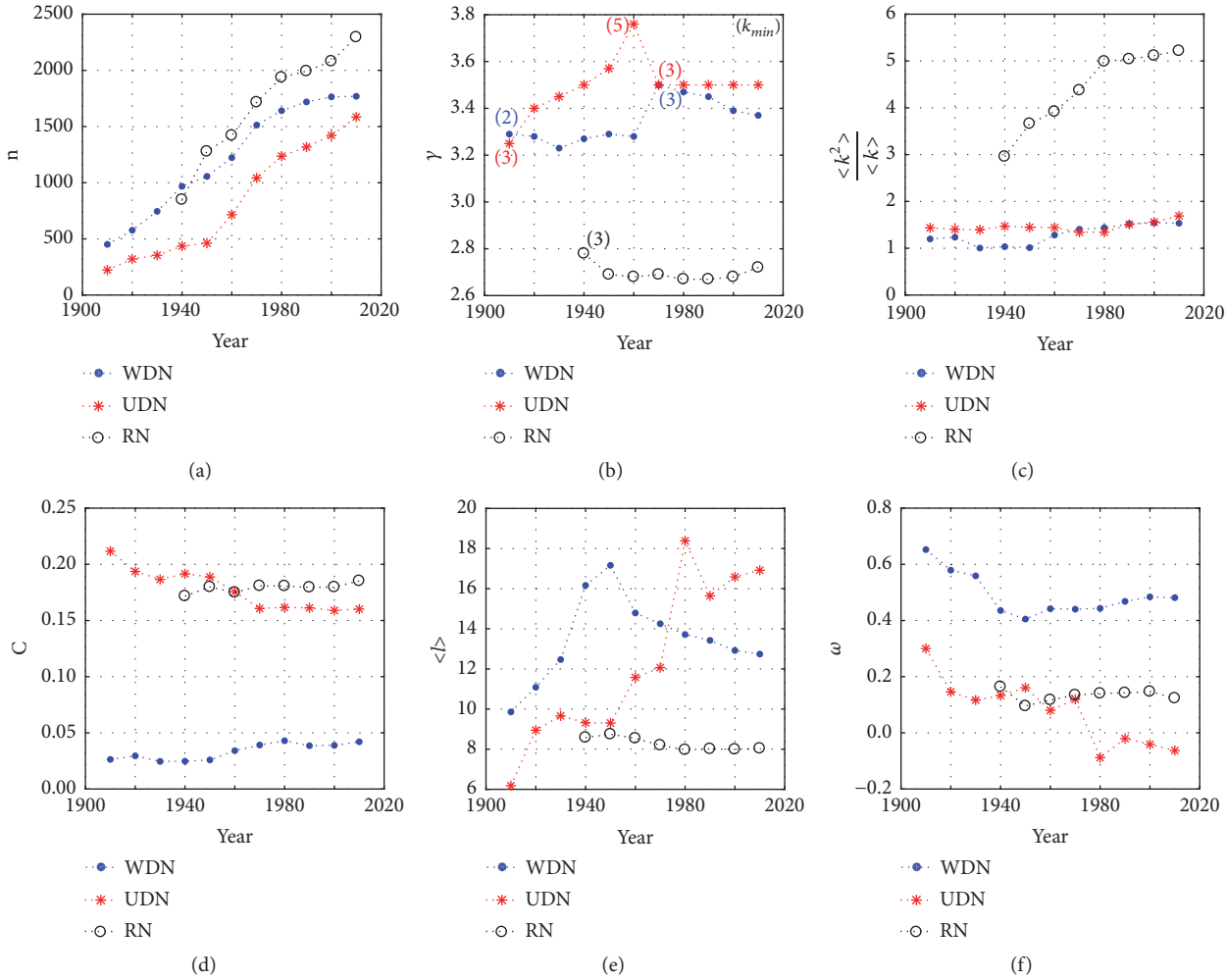

FIGURE 6: Topological properties of coevolving WDN, UDN, and RN: (a) number of vertices n; (b) power-law exponent γ; (c) dispersion index; (d) clustering coefficient C; (e) characteristic path length $\langle l \rangle$; and (f) small worldness ω.

identified for the WDN (see p values ≥ 0.1 in Appendix A). According to Achard et al. [36] the extent to which these distributions fit a power-law can be a useful indicator of network resilience. Furthermore, when comparing γ with previous studies in the literature, similar ranges between 2 and 4 are reported [17, 20, 21].

In this study, the lowest exponents γ are reported for the RN compared to those for the WDN and UDN. Peaks of γ for the WDN and UDN can be explained with the tree-like expansion of the network to new parts of the city and without a strong network densification at those times (see description in Table 1). During the last part of the 20th century the γ for the WDN tends to decrease, whereas the UDN and RN evolution is characterized by a network growth with a nearly constant power-law exponent γ. This could indicate that the networks are now topologically "mature"; i.e., a similar behavior is expected when the network grows further. The ratios of variance $\langle k^2 \rangle$ and the mean $\langle k \rangle$ of the node degrees are illustrated in Figure 6(c). For WDN and UDN it is nearly constant during their evolution $[1 \leq D \leq 2]$. An increasing bilinear trend of dispersion is observed for the RN, indicating the preferential attachment tendencies of new nodes to already well connected nodes. All networks show dispersion indices greater than 1 and thus exceed the value of expected random graphs following a Poisson distribution ($D = 1$).

As a measure of functional segregation (local efficiency), high average clustering coefficients describe the presents of cliques, where neighboring nodes are well connected among each other. During the last half of the century, C remained nearly constant for all infrastructure networks, with highest values for the RN, followed by UDN and WDN at year 2010.

The characteristic path length $\langle l \rangle$ of the network states in dual representation is shown in Figure 6(e). In the dual representation, the path length defines the number of changing edge attributes (e.g., diameter changes) between two dual vertices. Small $\langle l \rangle$ indicate a global efficiency meaning that every vertex is connected to every other through a short distance. In general, $\langle l \rangle$ increases with expanding geographical boundaries of the network (Figure 2). During the 1980s there is a significant increase of $\langle l \rangle$ for the UDN, possibly because of the tree-like connections of peripheral zones and neighboring villages to the central wastewater treatment plant. In contrast, $\langle l \rangle$ for the WDN decreases

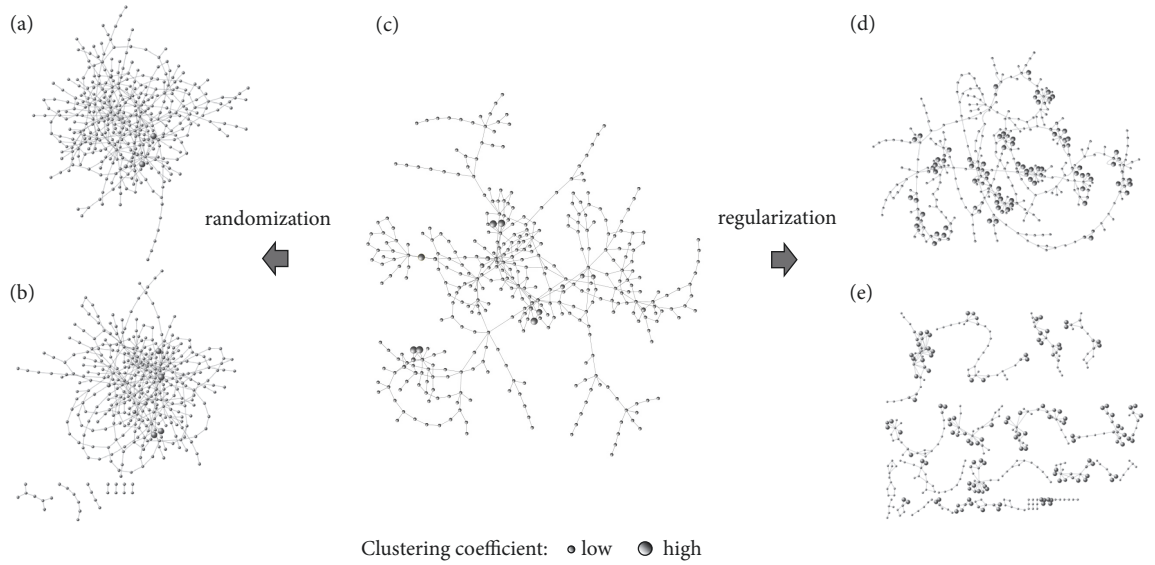

FIGURE 7: Creation of the equivalent random and regular lattice networks (same node degree distribution) by edge rewiring to test the small worldness. (a)-(b) Randomized networks with and without maintaining connectivity; (c) LLC of the dual mapped WDN 1910; (d)-(e) the lattice equivalents with and without maintaining connectivity.

during the past few years, as a result of the WDN densification and the construction of alternative flow paths for redundancy purposes. Furthermore, it is remarkable that $\langle l \rangle$ for the UDNs at the early stages of the 20th century is lower compared to that for WDNs. One reason for that is that the UDN at the historical center of the Alpine city had fewer alterations of conduit diameters (see Figure 2, middle left), resulting from the coarse design concepts and material limitations at that time. As the road network grows over time, we observe the lowest values for $\langle l \rangle$ are nearly constant trend over time, indicating a high network integrity.

Figure 6(f) provides a quantitative measure of the small-world properties ω over a spectrum of network topologies. Telesford et al. [31] describe ω in proximity to zero as small-world network; however, no sharp boundary of the small-world region exists. Positive ω indicate a graph with more random characteristics, as we observe for all infrastructure during the first half of the 20th century. However, over time, the networks tend to become less random and closer to small worldness. While ω is always larger than 0.40 for the WDN, UDN and RN have $|\omega|$- values less than 0.16 after the first network state. Therefore, we claim the small-world property of UDN and RN, while the former in recent decades can be considered as the closest to the small-world optimum.

Figure 7 shows an example of the random and regular lattice equivalents for the WDN 1910, needed to determine the small worldness. By preserving the same node degree distribution, edges of the initial network (see Figure 7(c)) are rewired in a stochastic process [37, 38]. Differences between the networks in Figures 7(a) and 7(b), as well as in Figures 7(d) and 7(e), are the preservation of the network connectivity. The effective number of rewiring per edge for creating the network equivalents is around 10 (for the regularization approximately 100 times more iterations needed), determined though parameter convergence (see Appendix C).

Previous studies have shown that understanding the network structure gives insights to vulnerabilities and structural resilience of the systems (i.e., scale-free networks are found to be highly resilient against random failure but vulnerable to targeted attacks) [9, 39]. Implications to the infrastructure management could, for example, relate to system operation to emphasize special protection or increased maintenance of critical network components ("hubs"). While this is relatively obvious at key points (such as water or wastewater treatment plants), in most cases less attention has been paid to individual pipe sections due to their complexity. A first step towards more resilient networks is already proposed by Mair et al. [40] and Zischg et al. [41], to use a "less-critical" subset of the colocated road network with strong similarities to generate possible WDNs. Second, when considering all infrastructure networks as an entire system ("multiplex network"), severe failure cascades through the network layers should be prevented through avoiding certain interlayer links (e.g., co-location of "hubs") [42]. Resulting resilient infrastructure systems should be capable of minimizing the failure impacts and a fast recovery to a stable system state [11]. While the former factor certainly depends on the (multiplex) network topology and on the type of network disruption (see e.g., [43, 44]), for the latter one several influencing factors exist, which in most cases are more difficult to quantify (e.g., resources availability, societal needs, preparedness actions, economy adjustments, etc.) [6]. However, the assessment of infrastructure system resilience goes beyond the scope of this study.

4.4. Remapping from Dual to Primal Space. Remapping the dual graph characteristics to the primal graph representation allows for georeferenced visualization and further spatial

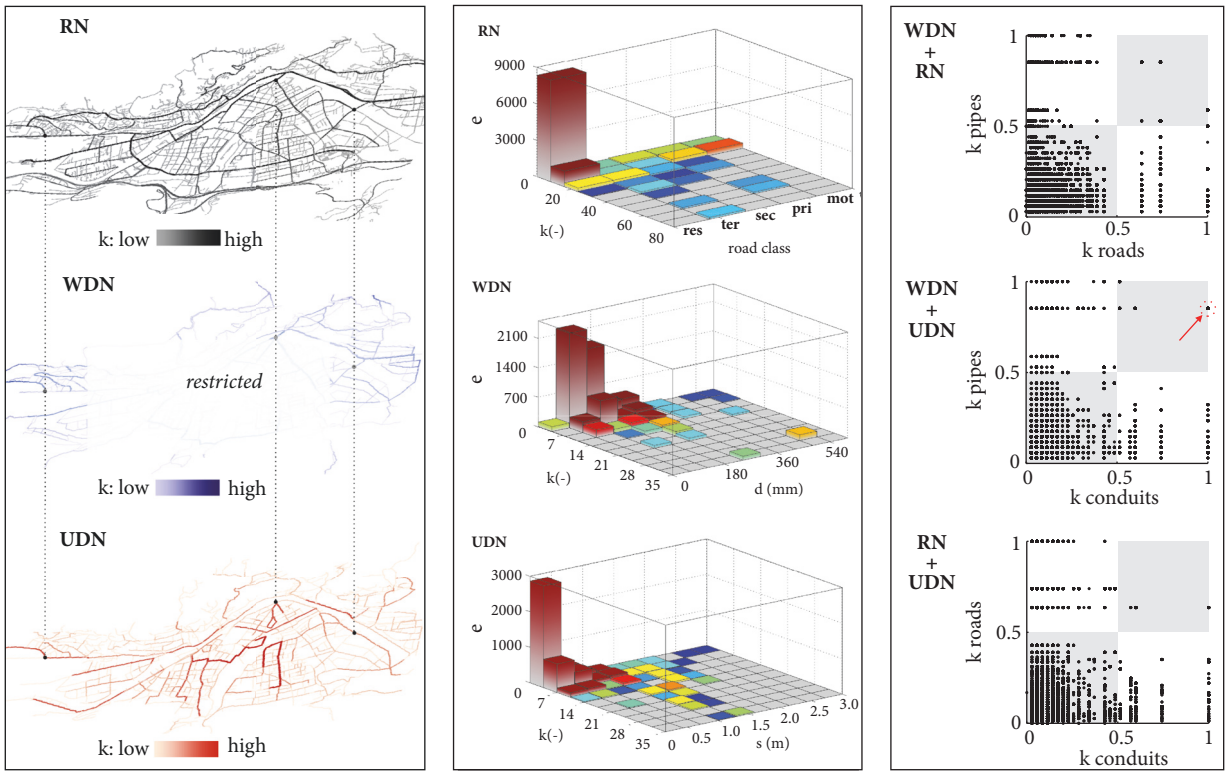

(a) (b) (c)

Figure 8: Remapping of the dual (node) degree to the primal space for WDN, UDN, and RN. (a) Remapped dual degree; (b) correlation analysis between dual degree and functional edge class describing flow capacity: e is the number of primal edges and the road classes represent residential (**res**), tertiary (**ter**), secondary (**sec**), and primary (**pri**) roads and motorways (**mot**); and (c) co-location of dual degree among different network types.

analyses among the different network types. Figure 8(a) shows the example of remapping the dual (node) degree to the original physical embedded infrastructure networks at year 2010. The highlighted bold edges represent the dual network "hubs", i.e., the elements with the most interconnections. In case those elements fail, the network gets easily fragmented, making for example the emergency supply very difficult through the central WDN. A comparison of the dual degree and the edge class (pipe diameter, conduit size, and road type) shows that they do not necessarily correlate. This implies that edges with the highest capacity (large diameter in WDN, large conduits sizes in UDN, and motorways (mot) in the RN) do not have the most intersections.

For the RN the "high degree hubs" are identified to be tertiary and primary roads. The reason for this finding for the WDN and UDN is that the source and sink nodes (water sources and WWTP) are located outside the city, requiring "high capacity transmission edges" to the inner parts of the network, which usually have fewer connections. However, low degree "terminal dual nodes" are mostly found in the edge classes with the lowest capacity (see bivariate histograms in Figure 8(b)).

4.5. Geospatial Co-location. We present the results of the geospatial co-location analysis to identify the spatial relationships of dual node degrees among the three network types. Mair et al. [22] found that approximately 90% of the WDN and UDN are located below the RN for this case study, however without considering their topological characteristics. Here we pairwise compare the normalized dual (node) degrees of the colocated infrastructure networks (see Figure 8(c)). Nodes in the upper right corner of the scatter plots indicate that high node degree components of both networks are colocated. For example, one conduit segment (UDN) with the highest k is colocated with one pipe segment (WDN) with the second highest k (indicated with the arrow and a red circular marker). This could be an indicator for an increased cascading vulnerability when failures occur across multiple networks.

These findings provide a first step towards the assessment of structural resilience and network interdependencies. Besides the identification of the "connectors" (high connectivity nodes), the "carriers" (high capacity node) should be further addressed. One future direction of this work could be the analysis of cascading failure across multiple network layers (e.g., a pipe break occurs which affects the water supply but also influences the colocated road and urban drainage network parts due to traffic rerouting and additional inflow to sewers). These analyses could provide helpful insights in the resilient (re)design of networks, providing an integrated view across the usually separated systems.

Table 2: Statistical tests of the small world (C: average clustering coefficient; $\langle l \rangle$: characteristic path length; and ω: ratio indicating the small-world property) and power-law hypotheses (γ: scaling parameter; k_{min}: lower bound for curve fitting; p value: goodness-of-fit for power-law hypothesis) over time for the WDN, UDN, and RN according to Telesford et al. [31] and Clauset et al. [24].

Year	C			$\langle l \rangle$			ω			$\gamma(k_{min})$			p value		
	WDN	UDN	RN	WDN	UDN	RN	WDN	UDN	RN	WDN	UDN	RN	WDN	UDN	RN
1910	0.026	0.212	-	9.86	6.18	-	0.652	0.300	-	3.29 (2)	3.25 (3)	-	**0.158**	**0.169**	-
1920	0.030	0.194	-	11.09	8.95	-	0.579	0.146	-	3.28 (2)	3.40 (3)	-	**0.565**	**0.365**	-
1930	0.025	0.187	-	12.47	9.66	-	0.559	0.117	-	3.23 (2)	3.45 (3)	-	0.016	**0.518**	-
1940	0.025	0.192	0.172	16.16	9.32	8.58	0.436	0.133	0.164	3.27 (2)	3.50 (3)[3]	2.78 (3)	0.015	**0.754**	0.021
1950	0.026	0.189	0.180	17.16	9.30	8.75	0.405	0.161	0.095	3.29 (2)	3.57 (3)	2.69 (3)[2]	**0.102**	**0.348**	0.008
1960	0.034	0.176	0.175	14.79	11.58	8.54	0.442	0.080	0.117	3.28 (2)	3.76 (5)	2.68 (3)	0.084	**0.111**	0.038
1970	0.039	0.161	0.181	14.25	12.06	8.20	0.440	0.120	0.134	3.50 (3)	3.50 (3)[3]	2.69(3)	**0.187**	0.003	0.005
1980	0.043	0.162	0.181	13.71	18.38	7.97	0.443	-0.088	0.140	3.47 (3)	3.50 (3)[3]	2.67 (3)	**0.238**	0.004	0.010
1990	0.039	0.161	0.180	13.42	15.64	8.01	0.468	-0.020	0.142	3.45 (3)	3.50 (3)[3]	2.67 (3)	**0.791**	0.002	0.047
2000	0.039	0.159	0.180	12.92	16.59	7.99	0.484	-0.041	0.147	3.39 (3)	3.50 (3)[3]	2.68 (3)	**0.257**	0.001	**0.110**
2010	0.042	0.160	0.185	12.74	16.92	8.04	0.481	-0.063	0.123	3.37 (3)[1]	3.50 (3)[3]	2.72 (3)	0.051	0.002	**0.694**

[1,2,3] recalculated k_{min} to maximize p *value* from/to: = (5)/(3); (9)/(3); (4)/(3); p values ≥ 0.1 proving the power-law hypothesis are shown in **bold** (50% of the networks).

Table 3: Topological dual mapped properties (n: number of nodes; e: number of edges; $\langle k \rangle$: mean node degree; k_{max}: maximum node degree; and $\langle k^2 \rangle$: node degree variance) over time for the WDN, UDN, and RN.

Year	n			e			$\langle k \rangle$			k_{max}			$\langle k^2 \rangle$		
	WDN	UDN	RN	WDN	UDN	RN	WDN	UDN	RN	WDN	UDN	RN	WDN	UDN	RN
1910	451	223	-	535	356	-	2.37	3.19	-	15	16	-	2.84	4.59	-
1920	577	321	-	703	467	-	2.44	2.91	-	22	19	-	3.01	4.09	-
1930	745	354	-	907	510	-	2.43	2.88	-	14	19	-	2.45	4.02	-
1940	968	436	849	1,171	639	1,288	2.42	2.93	3.03	17	19	32	2.50	4.31	8.97
1950	1,056	462	1,278	1,284	676	1,868	2.43	2.93	2.92	17	19	52	2.46	4.24	10.70
1960	1,223	715	1,420	1,512	1,009	2,093	2.47	2.82	2.95	32	23	54	3.17	4.07	11.55
1970	1,513	1,042	1,716	1,913	1,441	2,575	2.53	2.77	3.00	37	22	65	3.55	3.71	13.13
1980	1,641	1,236	1,937	2,097	1,700	2,955	2.56	2.75	3.05	34	22	71	3.67	3.70	15.23
1990	1,719	1,318	1,993	2,203	1,821	3,040	2.56	2.76	3.05	34	30	74	3.90	4.17	15.37
2000	1,764	1,431	2,081	2,272	1,970	3,172	2.58	2.77	3.05	34	31	74	3.97	4.33	15.59
2010	1,769	1,585	2,295	2,293	2,226	3,479	2.59	2.81	3.03	34	35	74	3.98	4.75	15.82

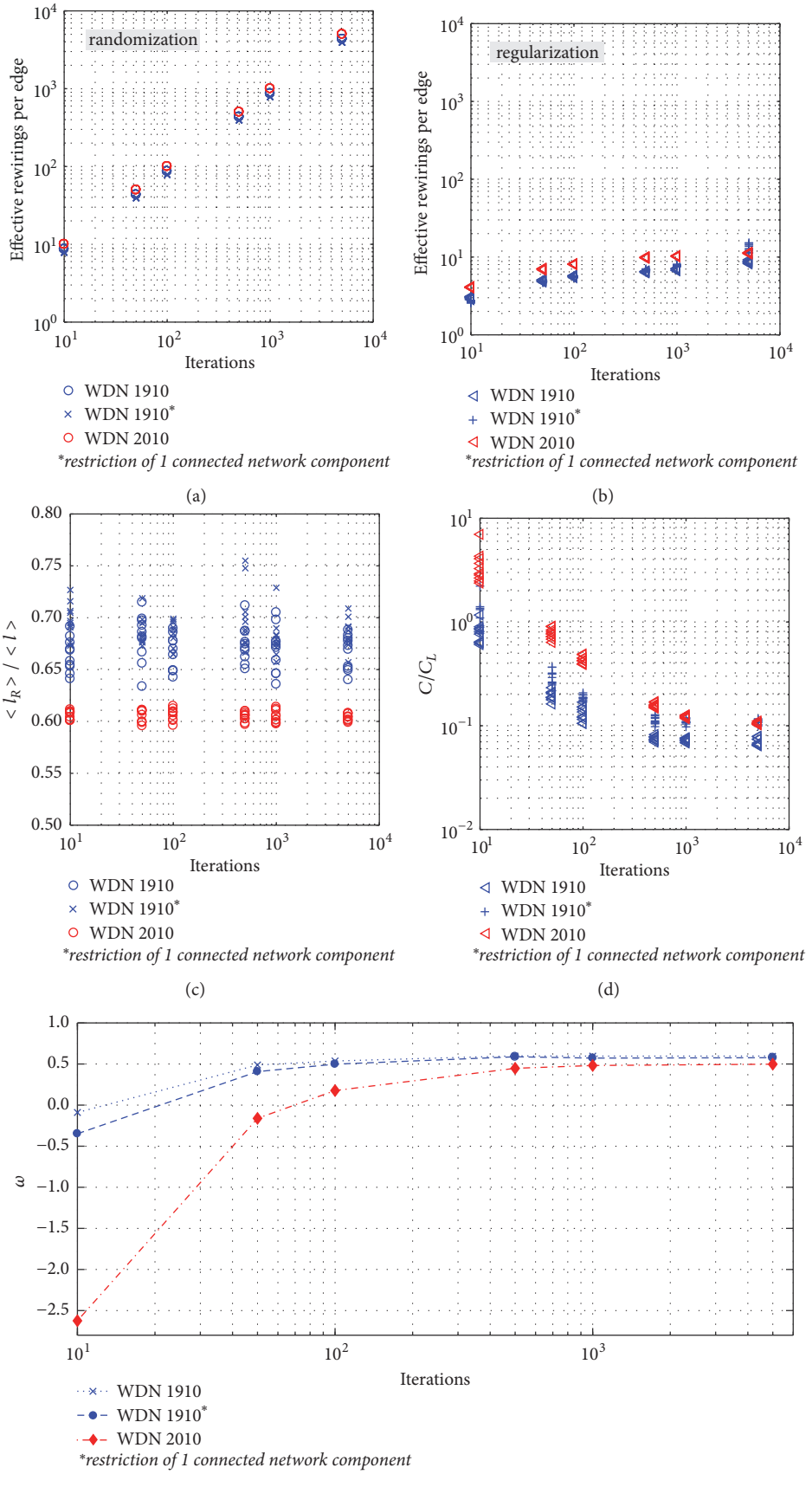

FIGURE 9: Convergence plots when creating the random and regular network equivalents (10 stochastic networks per iteration step) for the WDN 1910 and the WDN 2010. Effective edge rewiring in (a) the randomization process and (b) the regularization process; (c) ratio of the characteristic path length of the randomized and the original networks; (d) ratio of the clustering coefficient of the original and the regularized networks; and (e) the convergence of the small-world property ω. For further analysis the number of iterations was set to 10^1 and 10^3 for the randomization and regularization process, respectively.

5. Conclusions

The historical data set of water distribution, urban drainage, and road networks of an Alpine city was investigated using a dual mapping approach (Hierarchical Intersection Continuity Negotiation method) and complex network analysis metrics were estimated. From a sensitivity analysis for the angular threshold Θ_{max} using the HICN approach it is concluded that, unlike for road networks, where Θ_{max} also is a criterion for visibility, we suggest that restricting Θ_{max} in WDNs and UDNs is less important than finding and aggregating pipe segments with unique identity because of their underground locations.

The node degree distributions are heavy tailed with greater variance than expected for random networks. Across all three network types and for 50% of the time-stamped networks truncated [Pareto] power-law functions $P(k) \sim k^{-\gamma}$, $k \geq k_{min}$ (γ between 2.67 and 3.76; k_{min} mostly ranging between 2 and 3) were proven and were in the range of previous studies on urban infrastructure networks. While the RN tends towards a clear scale-free behavior during evolution, the opposite is observed for the UDN. No clear trends were identified for the WDN. All networks tend to fall in the small-world region characterized by high global and local efficiencies, during their spatiotemporal evolution. We conclude that similar to other "self-organized" networks, infrastructure networks in their dual representation can also exhibit scale-free properties and thus exhibit the failure dynamics typical of scale-free networks.

Previous studies showed that networks with highly variable node degree distributions, such as scale-free networks, are highly resilient to random failures but have high vulnerabilities to targeted attacks. Furthermore, the extent to which these distributions fit a power-law can be a useful indicator of network resilience. With the presented dual mapping methodology, patterns (e.g., vertex connectivity) and trends for the future infrastructure development were obtained. Furthermore, the reflected structural features, such as the "highly connected" components of the networks, were identified and remapped to the primal map. It was shown that the "highly connected" components do not necessarily correlate with "high capacity" components. Through the pairwise comparison of the dual degree of different network types, we identified the location where "high degree" components are colocated. These findings could be a measure of assessing the interdependencies and cascading vulnerabilities across multilayer networks.

Appendix

A.

See Table 2.

B.

See Table 3.

C.

See Figure 9.

Data Availability

(1) The current and historical georeferenced data of the water distribution and urban drainage networks, used to support the findings of this study, have not been made available because they are protected for security reasons. (2) The road network data which was used to support the findings of this study was taken from open street maps. (3) The dual mapped representation of the water distribution, urban drainage, and road networks, used to support the findings of this study, is available from the corresponding author upon request.

Conflicts of Interest

The authors declare that there are no conflicts of interest regarding the publication of this paper.

Acknowledgments

This work was initiated at the international synthesis workshop "Dynamics of Structure and Functions of Complex Networks", held at Korea University, Seoul, South Korea, during summer 2015. The authors gratefully acknowledge Sybille Glöckner, who provided the historical water distribution network, reconstructed during her master thesis. This research was partially funded by the Austrian Research Promotion Agency (FFG) within the research project ORONET [Project number: 858557], the Austrian Science Fund (FWF) [Project number: P 31104-N29], the Austrian Marshall Plan Foundation, and the NSF Collaborative Research RIPS Type 2: Resilient Simulation for Water, Power, and Road Networks [Project number: 1441188].

References

[1] P. Blanchard and D. Volchenkov, *Mathematical Analysis of Urban Spatial Networks*, Understanding Complex Systems, 1, Springer, Berlin, Germany, 2009.

[2] S. H. Strogatz, "Exploring complex networks," *Nature*, vol. 410, no. 6825, pp. 268–276, 2001.

[3] Y. Assenov, F. Ramírez, S.-E. Schelhorn, T. Lengauer, and M. Albrecht, "Computing topological parameters of biological networks," *Bioinformatics*, vol. 24, no. 2, pp. 282–284, 2008.

[4] M. C. González, C. A. Hidalgo, and A.-L. Barabási, "Understanding individual human mobility patterns," *Nature*, vol. 453, no. 7196, pp. 779–782, 2008.

[5] S. Uhlmann, H. Mannsperger, J. D. Zhang et al., "Global microRNA level regulation of EGFR-driven cell-cycle protein network in breast cancer," *Molecular Systems Biology*, vol. 8, article 570, 2012.

[6] D. A. Eisenberg, J. Park, and T. P. Seager, "Sociotechnical Network Analysis for Power Grid Resilience in South Korea," *Complexity*, vol. 2017, 14 pages, 2017.

[7] A. Barabasi and R. Albert, "Emergence of scaling in random networks," *Science*, vol. 286, no. 5439, pp. 509–512, 1999.

[8] A. P. Riascos, "Universal scaling of the distribution of land in urban areas," *Physical Review E: Statistical, Nonlinear, and Soft Matter Physics*, vol. 96, no. 3, Article ID 032302, 2017.

[9] K. A. Zweig and K. Zimmermann, "Wanderer between the worlds - Self-organized network stability in attack and random failure scenarios," in *Proceedings of the 2nd IEEE International Conference on Self-Adaptive and Self-Organizing Systems, SASO 2008*, pp. 309–318, Italy, October 2008.

[10] J. P. G. Sterbenz, E. K. Çetinkaya, M. A. Hameed, A. Jabbar, S. Qian, and J. P. Rohrer, "Evaluation of network resilience, survivability, and disruption tolerance: analysis, topology generation, simulation, and experimentation: Invited paper," *Telecommunication Systems*, vol. 52, no. 2, pp. 705–736, 2013.

[11] H. Klammler, P. S. C. Rao, and K. Hatfield, "Modeling dynamic resilience in coupled technological-social systems subjected to stochastic disturbance regimes," *Environment Systems and Decisions*, vol. 38, no. 1, pp. 140–159, 2018.

[12] A. Yazdani, R. A. Otoo, and P. Jeffrey, "Resilience enhancing expansion strategies for water distribution systems: a network theory approach," *Environmental Modelling & Software*, vol. 26, no. 12, pp. 1574–1582, 2011.

[13] A. Yazdani and P. Jeffrey, "Applying network theory to quantify the redundancy and structural robustness of water distribution systems," *Journal of Water Resources Planning and Management*, vol. 138, no. 2, pp. 153–161, 2012.

[14] F. Zeng, X. Li, and K. Li, "Modeling complexity in engineered infrastructure system: Water distribution network as an example," *Chaos: An Interdisciplinary Journal of Nonlinear Science*, vol. 27, no. 2, Article ID 023105, 2017.

[15] S. Porta, P. Crucitti, and V. Latora, "The network analysis of urban streets: a primal approach," *Environment and Planning B: Planning and Design*, vol. 33, no. 5, pp. 705–725, 2006.

[16] A. P. Masucci, K. Stanilov, and M. Batty, "Exploring the evolution of London's street network in the information space: A dual approach," *Physical Review E: Statistical, Nonlinear, and Soft Matter Physics*, vol. 89, no. 1, Article ID 012805, 2014.

[17] S. Porta, P. Crucitti, and V. Latora, "The network analysis of urban streets: A dual approach," *Physica A: Statistical Mechanics and its Applications*, vol. 369, no. 2, pp. 853–866, 2006.

[18] M. Hu, R. Jiang, R. Wang, and Q. Wu, "Urban traffic simulated from the dual representation: Flow, crisis and congestion," *Physics Letters A*, vol. 373, no. 23-24, pp. 2007–2011, 2009.

[19] H. Jun and G. V. Loganathan, "Valve-controlled segments in water distribution systems," *Journal of Water Resources Planning and Management*, vol. 133, no. 2, pp. 145–155, 2007.

[20] E. Krueger, C. Klinkhamer, C. Urich, X. Zhan, and P. S. C. Rao, "Generic patterns in the evolution of urban water networks: Evidence from a large Asian city," *Physical Review E: Statistical, Nonlinear, and Soft Matter Physics*, vol. 95, no. 3, Article ID 032312, 2017.

[21] C. Klinkhamer, E. Krueger, X. Zhan, F. Blumensaat, S. V. Ukkusuri, and P. S. C. Rao, Functionally Fractal Urban Networks: Geospatial Co-location and Homogeneity of Infrastructure, 2017, https://export.arxiv.org/abs/1712.03883v1.

[22] M. Mair, J. Zischg, W. Rauch, and R. Sitzenfrei, "Where to find water pipes and sewers?-On the correlation of infrastructure networks in the urban environment," *Water (Switzerland)*, vol. 9, no. 2, p. 146, 2017.

[23] J. Zischg, *Understanding patterns, dependencies and resilience in complex urban water infrastructure networks*, 2018, https://static1.squarespace.com/static/559921a3e4b02c1d7480f8f4/t/5af00302758d4670efbdc46d/1525678950226/Zischg+Jonatan_782.pdf.

[24] A. Clauset, C. R. Shalizi, and M. E. Newman, "Power-law distributions in empirical data," *SIAM Review*, vol. 51, no. 4, pp. 661–703, 2009.

[25] Á. Corral and Á. González, Power-law distributions in geoscience revisited, https://arxiv.or/pdf/1810.07868.pdf, 2018.

[26] M. Barthélemy, "Spatial networks," *Physics Reports*, vol. 499, no. 1–3, pp. 1–101, 2011.

[27] E. Weisstein, "Pareto distribution," in *mathworld–a wolfram web resource*, 2018, http://mathworld.wolfram.com/ParetoDistribution.html.

[28] J. Zischg, C. Klinkhamer, X. Zhan et al., "Evolution of Complex Network Topologies in Urban Water Infrastructure," in *Proceedings of the 17th World Environmental and Water Resources Congress 2017*, pp. 648–659, USA, May 2017.

[29] P. Shannon, A. Markiel, O. Ozier et al., "Cytoscape: a software Environment for integrated models of biomolecular interaction networks," *Genome Research*, vol. 13, no. 11, pp. 2498–2504, 2003.

[30] D. J. Watts and S. H. Strogatz, "Collective dynamics of "small-world" networks," *Nature*, vol. 393, no. 6684, pp. 440–442, 1998.

[31] Q. K. Telesford, K. E. Joyce, S. Hayasaka, J. H. Burdette, and P. J. Laurienti, "The Ubiquity of Small-World Networks," *Brain Connectivity*, vol. 1, no. 5, pp. 367–375, 2011.

[32] R. Sitzenfrei, M. Mair, F. Tscheikner-Gratl, B. Hupfauf, and W. Rauch, "What can we learn from historical water network transition?" in *Proceedings of the World Environmental and Water Resources Congress 2015: Floods, Droughts, and Ecosystems*, pp. 907–916, USA, May 2015.

[33] S. Gloeckner, *Die Historie der Hochdruckwasserversorgungsanlage in Innsbruck - Hydraulische Modellierung und Ausblick (in German) [Master Thesis]*, University of Innsbruck, Innsbruck, Austria, 2017.

[34] M. Schulze, *Historische entwicklung der kanalisation innsbrucks und die entwicklung der technischen regelwerke (in German)*, University of Innsbruck, Innsbruck, Austria, 2012.

[35] X. Zhan, S. V. Ukkusuri, and P. S. Rao, "Dynamics of functional failures and recovery in complex road networks," *Physical Review E: Statistical, Nonlinear, and Soft Matter Physics*, vol. 96, no. 5, 2017.

[36] S. Achard, R. Salvador, B. Whitcher, J. Suckling, and E. Bullmore, "A resilient, low-frequency, small-world human brain functional network with highly connected association cortical hubs," *The Journal of Neuroscience*, vol. 26, no. 1, pp. 63–72, 2006.

[37] M. Rubinov and O. Sporns, "Complex network measures of brain connectivity: Uses and interpretations," *NeuroImage*, vol. 52, no. 3, pp. 1059–1069, 2010.

[38] S. Maslov and K. Sneppen, "Specificity and stability in topology of protein networks," *Science*, vol. 296, no. 5569, pp. 910–913, 2002.

[39] Z. J. Bao, Y. J. Cao, L. J. Ding, and G. Z. Wang, "Comparison of cascading failures in small-world and scale-free networks subject to vertex and edge attacks," *Physica A: Statistical Mechanics and its Applications*, vol. 388, no. 20, pp. 4491–4498, 2009.

[40] M. Mair, W. Rauch, and R. Sitzenfrei, "Spanning Tree-Based Algorithm for Generating Water Distribution Network Sets by Using Street Network Data Sets," in *Proceedings of the World Environmental and Water Resources Congress 2014: Water Without Borders*, pp. 465–474, USA, June 2014.

[41] J. Zischg, W. Rauch, and R. Sitzenfrei, "Morphogenesis of Urban Water Distribution Networks: A Spatiotemporal Planning Approach for Cost-Efficient and Reliable Supply," *Entropy*, vol. 20, no. 9, p. 708, 2018.

[42] S. V. Buldyrev, R. Parshani, G. Paul, H. E. Stanley, and S. Havlin, "Catastrophic cascade of failures in interdependent networks," *Nature*, vol. 464, no. 7291, pp. 1025–1028, 2010.

[43] C. D. Brummitt, R. M. D'Souza, and E. A. Leicht, "Suppressing cascades of load in interdependent networks," *Proceedings of the National Acadamy of Sciences of the United States of America*, vol. 109, no. 12, pp. E680–E689, 2012.

[44] A. Vespignani, "Complex networks: The fragility of interdependency," *Nature*, vol. 464, no. 7291, pp. 984-985, 2010.